EUROPEAN COOPERATION
IN SCIENCE
AND TECHNOLOGY

EURO-COST

CA20120 TD(22)02029
Lyon, France
June 13-15, 2022

SOURCE: EURECOM, Sophia Antipolis, France

5GNR Indoor Positioning By Joint DL-TDoA and DL-AoD

Mohsen Ahadi, Florian Kaltenberger

EURECOM
Campus SophiaTech
450 route des Chappes
06410 BIOT
Phone: +33 4 93 00 81 86
Fax: +33 4 93 00 82 00
Email: florian.kaltenberger@eurecom.fr

5GNR Indoor Positioning By Joint DL-TDoA and DL-AoD

1st Mohsen Ahadi
Communication Systems Department
EURECOM
Sophia Antipolis, France
mohsen.ahadi@eurecom.fr

2nd Florian Kaltenberger
Communication Systems Department
EURECOM
Sophia Antipolis, France
florian.kaltenberger@eurecom.fr

***Abstract*—The topic of indoor positioning of a user terminal is becoming increasingly significant in the context of mobile networks as accurate localization based on global navigation satellite systems (GNSS) is not possible inside buildings. The 5G New Radio (NR) networks based on the 3GPP have introduced several enhanced features to allow the accurate positioning of user terminals. By utilizing mmWave for the downlink positioning reference signals (DL-PRS) in a 3GPP Rel-16 5G NR system in Frequency Range 2 (FR2), we investigate the performance of a combined method consisting of Downlink Time Difference of Arrival (DL-TDoA) and Downlink Angle of Departure (DL-AoD). TDoA is a widely used horizontal positioning technique that does not require tight synchronization between base stations and mobile stations. Moreover, Multiple antennas beamforming on base stations leads to high vertical positioning accuracy with AoD. We use ray-tracing-based site-specific channel models to evaluate our joint positioning algorithm's performance in an Indoor Factory (InF) scenario. The simulation results show sub-meter user localization error which is a significant improvement compared to applying the previous methods separately.**

***Index Terms*—Positioning, Time Difference of Arrival, Angle of Departure, Position Estimation, Beamforming, 5G New Radio.**

I. Introduction

Location information of mobile devices provides valuable data that can be exploited for new services and applications, for example, Industry 4.0 and the Internet of Things (IoT). This information may also be used to support wireless operators to enhance network performance [1]. However, a precise position estimation based on GNSS is not possible for indoor scenarios where no Line of Sight (LOS) to a satellite is available. 5G-NR Stand Alone (SA) networks propose mmWave in FR2 which enables wideband signals, low latency, beamforming, and precise angle estimation with multiple antennas. These possibilities in combination with the 5GNR positioning architecture can be exploited for an accurate indoor positioning system. Several well-known positioning techniques have been proposed for determining the position of a point: Time of Arrival (ToA) [2], [3] Time Difference of Arrival (TDoA), Received Signal Strength (RSS), and Direction of Arrival [4] and Departure. (also known as Angle of Arrival and Angle of Departure) Although ToA-based positioning results in a proper horizontal accuracy along the x, and y-axis, it requires highly accurate clock synchronization among all Base Stations (BSs) and mobile devices. RSS-based techniques [5], [6], are very sensitive to fast and slow fading and tend to provide only rough localization estimates. On the other hand, TDoA systems avoid the requirements of clock synchronization at the point of interest or tag-end by considering the different arrival times of signals that originate at two distinct reference points [7]. The time difference calculation at the mobile avoids synchronization requirements between the mobile and the BSs. Note that TDoA-based positioning schemes still require clock synchronization between all the BSs in the system. Thus, excluding synchronization issues, the sources of error of TDoA-based systems are the same as the ones existing for ToA schemes. The utilization of antenna arrays on the transmitter or receiver, allows the angle parameters to be measured and exploited for high positioning precision especially vertical. Time and angle-based positioning have been pursued in many previous research works separately. The authors of [8] propose a geometric approach for positioning problems, but optimization is not considered. In the papers [9]- [12], refinements for TDoA- based positioning algorithms are proposed to make the position estimations robust. However, the practical implementation is not well-considered, and neither are simulations in realistic environments. They also assume (in the simulations) that all the TDoA (or ToA) estimates have the same statistical characteristics, which is not the case in practice. In [13], a simple minimum least squared method is used to estimate the user's coordinates based on DL-AoD. In other related works, finding the UE position depends on measuring AoA which requires the UE to have a multi-antenna array. This is not feasible for every type of equipment such as mobile devices. Therefore, we propose using DL-AoD which is reported from gNBs to UE over network protocols [14] without requiring a large antenna array on the user terminal. Also, creating a joint TDoA-AOD positioning estimation algorithm for an indoor scenario with no GNSS LOS is presented for precise UE self-positioning. The novelty of this paper is applying a joint DL-TDoA and DL-AOD positioning algorithm with sub-meter accuracy performance in both horizontal and vertical planes, without a large antenna array requirement on the UE. In the following sections, we will go through the latest 5G positioning enhancements in architecture, signals, and measurements. Moreover, we demonstrate possible positioning accuracy with these new capabilities.

II. 5G POSITIONING ARCHITECTURE AND PROTOCOLS

A. RAN and Core Network Architecture

The 5G positioning architecture in the Release 16 [14] follows the LTE positioning model by introducing new entities in the 5G Next Generation Radio Access Network (5G-RAN) and the 5G Core Network (5GC) depicted in figure 1. LTE Positioning Protocol (LPP) is used as a communication protocol between the UE and the Location Management Function (LMF) via Access Mobility Function (AMF) in the 5GC. Moreover, signaling between gNB and LMF is obtained over New Generation Positioning Protocol A (NRPPa). Multiple antennas on gNBs and the availability of mm-Wave in 5G NR, enable the measurement of Downlink Angle of Departure (DL-AoD) as supporting information for UE to localize itself. This is a new on-demand System Information (SI) procedure, a UE can request positioning System Information Blocks (posSIBs) including the coordinate of the transmitting antennas as well as the beam angle information. The gNB provides this information to LMF over NRPPa. For DL-AoD estimation, UE measures the DL-PRS beams Reference Signal Received Power (RSRP). Moreover, By performing a Reference Signal Time Difference (RSTD) estimation on determined beams with the highest power from multiple gNBs, UE measures DL-TDoA of DL-PRS resources [15]. Based on PRS DL-TDoA, DL-AoD, and the geographical coordinates of the gNBs shared by LMF, UE can estimate its position. In section V we demonstrate how to jointly use angle and time parameters along with the geographical coordinates of the gNBs to estimate the UE position accurately in horizontal and vertical.

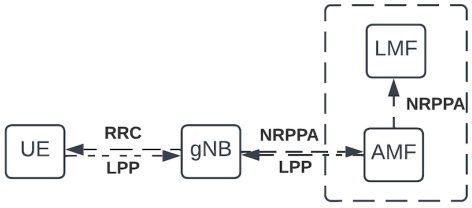

Fig. 1. 5GNR Positioning Architecture

B. Positioning Reference Signal

1) PRS Resource Set and Resources

One positioning frequency layer is made of one or more PRS resource sets distributed over one or more sites, all of which use the same carrier frequency and OFDM numerology. Each PRS resource in a resource set corresponds to a beam from a single location. When configuring a device to measure on a specific PRS resource in a PRS resource set, the location server learns not only which site the reported measurements for this PRS resource set belong to, but also the specific beam from that site [16].

2) PRS Comb Size

PRS setup enables permuted staggered comb. In this application, permuted indicates that the comb in each OFDM symbol has a distinct offset in the frequency domain. The comb factor can be adjusted to 2, 4, 6, or 12 sub-carriers, which means that the comb is used on every 2nd to every 12th sub-carrier. Using various combs, numerous simultaneous PRSs may be multiplexed.

3) PRS Bandwidth

A PRS resource in the frequency domain can be configured to have a bandwidth of up to 264 resource blocks (400MHz) in FR2, with all PRS resources in a PRS resource set having the same bandwidth and frequency domain location. In the time domain, one PRS resource is represented by two, four, six, or twelve OFDM signals.

III. AOD Estimation

A. Phased Antenna Array

Uniform Rectangular Array (URA) is a system of identical antenna elements. Array elements are distributed in the yz-plane in a rectangular lattice. The array boresight is along the x-axis. In this paper, we used a 2×2 and a 4×4 transmit antenna arrays which provide 4 and 16 beams respectively. To estimate the AOD, each gNB goes through a beam training process with a codebook containing a set of codewords $C^P = \{\mathbf{w}^1, ..., \mathbf{w}^P\}$ [17]. Therefore, a coarse estimation for the AOD of the propagation path is described as:

$$p^* = \arg\max_{p \in \mathcal{P}} A^p \tag{1}$$

where the beam with codeword $\mathbf{w}^p(\theta, \phi)$ maximizes the received power A^p on the UE. Without considering the noise, the ideal received signal strength is given by:

$$A^p = \sqrt{\left(\mathbf{h}\mathbf{w}^p\left(\theta,\phi\right)\right)^H \left(\mathbf{h}\mathbf{w}^p\left(\theta,\phi\right)\right)} \tag{2}$$

Thus, A^p can be used to estimate the beam index that refers to the elevation (θ), and azimuth (ϕ) of departure [17].

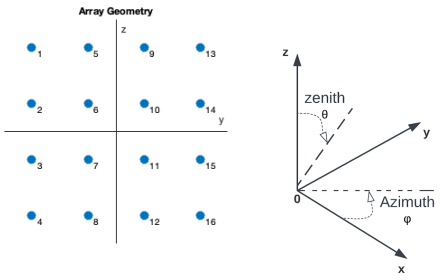

Fig. 2. Array geometry and coordinate system

B. Beamforming

Beam management is a set of Layer 1 (physical) and Layer 2 (medium access control) procedures to acquire and maintain a set of beam pair links [18] (a beam used at gNB paired with a beam used at UE). Beam sweeping is necessary at both transmit/receive point (TRP) side and UE side to establish a beam pair link. To accomplish gNB beam sweeping, analog beamforming on each PRS resource is used. The azimuth and elevation directions for the various beams are determined based on the number of antenna elements and the given sweep ranges. The particular PRS resource is then beamformed in each of these directions on the downlink. The transmitted

beamformed PRS waveform is received sequentially across each receive beam for receive-end beam sweeping. In general, for N transmit beams and M receive beams, each of the N beams is sent M times from gNB, so that each transmit beam is received over the M receive beams. For instance, from a TX antenna array of size 4×4 that we used here, we have a combination of 16 pairs of [azimuth, elevation] degrees to transmit the DL-PRS in (-45:45) degrees in azimuth and (-45:0) degrees in elevation. For a wave propagation in a direction described by the [azimuth, elevation] coordinates, the wave-vector k is given by:

$$\mathbf{k}(\theta, \phi) = (k_x, k_y, k_z) = \frac{2\pi}{\lambda}(\sin\theta\cos\phi, \sin\theta\sin\phi, \cos\theta) \tag{3}$$

Having N elements in an antenna array, with element i in a given location:

$$\mathbf{r}_i = (x_i, y_i, z_i) \tag{4}$$

A steering vector represents the set of phase delays for an incoming wave at each sensor element. For a plane wave that is described by a wave vector k, with N elements in an antenna array, steering vector $w(k)$ is an $N \times 1$ complex vector representing the relative phases at each antenna and is given by:

$$\mathbf{w}(\theta, \phi) = \left[\ e^{-j\mathbf{k}\cdot\mathbf{r}_1}, e^{-j\mathbf{k}\cdot\mathbf{r}_2}, \ldots, e^{-j\mathbf{k}\cdot\mathbf{r}_M}\ \right]^T \tag{5}$$

Each PRS resource transmitting wave will be multiplied by its corresponding steering vector to form a beam in a particular direction in space.

C. RSRP Measurement

After the dual-end sweep has been completed over TX and RX antennas, the best beam-pair link based on the highest RSRP measurement has to be determined. In this case with a single UE antenna, a TX beam has to be determined. The DL-PRS Reference Signal Received Power (DL-PRS-RSRP) is calculated as the linear average of power contributions of resource elements that are configured to carry DL-PRS reference signals. Within the NR Frequency Range 2 (FR2), DL PRS-RSRP is determined by combining the signals from antenna elements within a given receiver branch [20].

IV. TDoA Estimation

Based on the RSRP measurements, the pair of TX and RX beams have been identified for further processing of the TDoA. The time difference calculation on the UE avoids exact time synchronization requirements to the gNB. Note that TDoA-based positioning schemes still require clock synchronization between all the gNBs in the system and frequency synchronization between UE and gNBs. The DL reference signal time difference (DL-RSTD) [20] is the downlink relative timing difference between positioning node n and reference positioning node 1 to be assumed. In frequency range 2, the antenna of the UE shall be the reference point for the DL-RSTD.

A. Channel Estimation

To measure the DL-TDoA based on PRS resources, a channel estimation algorithm is used to calculate the timing offset between the reception and transmission of PRS resources. As Channel Estimation in OFDM Systems describes [21], the least-squares estimates of the channel frequency response at the pilot symbols are computed. To minimize any undesired noise from the pilot symbols, the least squares estimates are then averaged across time, then frequency bandwidth, with a growing window size that is proportional to the channel coherence time. Later, the findings will be interpolated over the whole sub-carriers in the bandwidth. In the next step, the frequency domain channel estimation is converted into an impulse response using an inverse Fourier transform. This result leaves us with some peaks which show when in time we received positioning reference signals. In this stage, As UE is synchronized with one of the gNBs, the timing difference between the provided channel estimation peaks is considered as the time difference of arrival or TDoA.

V. Joint AoD-TDoA Position Estimation

The trigonometric function of the estimated azimuth and zenith ($90° -$ elevation) angle of departure, as well as the range difference between the gNBs, are used in the positioning equations to compute the unknown UE coordinates. Taking (x, y, z) as the coordinate of the UE, the system of location equations can be written in a vector as follows:

$$\mathbf{f}(x, y, z) + \mathbf{e} = \mathbf{r} \tag{6}$$

where $\mathbf{f}$ contains $(3N-1)$ equations for N gNBs (with $2N$ angle, and $N-1$ time observations):

$$f_{AoD,2n-1}(x, y, z) = \cos(\theta_n) = \frac{(z - z_n)}{\sqrt{(x-x_n)^2 + (y-y_n)^2 + (z-z_n)^2}} \tag{7}$$

$$f_{AoD,2n}(x, y, z) = \sin(\varphi_n) = \frac{(y - y_n)}{\sqrt{(x-x_n)^2 + (y-y_n)^2}} \tag{8}$$

$$f_{TDoA,n}(x, y, z) = d_n - d_1 = \sqrt{(x-x_n)^2 + (y-y_n)^2} - \sqrt{(x-x_1)^2 + (y-y_1)^2} \tag{9}$$

In the above equations, (x_n, y_n, z_n) is the n^{th} gNB coordinate and d_n is the distance between the n^{th} gNB and UE for $n > 1$ in $f_{TDoA,n}$. Here d_1 is the reference gNB that the UE is synchronized to and has the strongest received signal which is assumed to be the nearest gNB with a LOS.

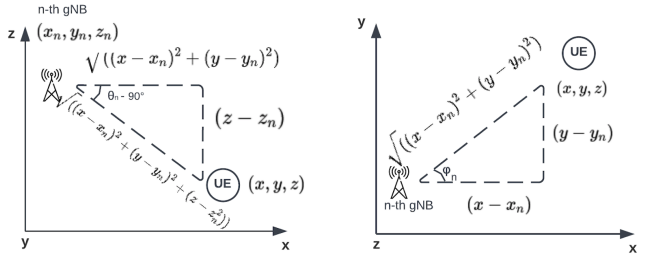

Fig. 3. Zenith and azimuth angle of departure

A. Taylor's Series Decomposition

The set of non-linear equations (7)-(9) at the point $(x^{(i)}, y^{(i)}, z^{(i)})$ can be solved by applying a Taylor series decomposition and limiting it by a linear term [22], as below;

$$\mathbf{f}(x, y, z) = \mathbf{f}\left(x^{(i)}, y^{(i)}, z^{(i)}\right) + \mathbf{D}^{(i)}\left(\mathbf{x} - \mathbf{x}^{(i)}\right), \tag{10}$$

where $\mathbf{D^{(i)}}$ is the $(3N-1)\times 3$ differential matrix estimated at the point $(x^{(i)}, y^{(i)}, z^{(i)})$, $\mathbf{x}$ is the 3 × 1 UE coordinate vector, and $\mathbf{x}^{(i)}$ is the 3 × 1 coordinate vector estimated at the point $(x^{(i)}, y^{(i)}, z^{(i)})$.

$$D^{(i)} = \begin{bmatrix} \frac{\partial f^{(i)}_{AoD,1}}{\partial x} & \frac{\partial f^{(i)}_{AoD,1}}{\partial y} & \frac{\partial f^{(i)}_{AoD,1}}{\partial z} \\ \vdots & \vdots & \vdots \\ \frac{\partial f^{(i)}_{AoD,2n}}{\partial x} & \frac{\partial f^{(i)}_{AoD,2n}}{\partial y} & \frac{\partial f^{(i)}_{AoD,2n}}{\partial z} \\ \frac{\partial f^{(i)}_{TDoA,2}}{\partial x} & \frac{\partial f^{(i)}_{TDoA,2}}{\partial y} & \frac{\partial f^{(i)}_{TDoA,2}}{\partial z} \\ \vdots & \vdots & \vdots \\ \frac{\partial f^{(i)}_{TDoA,n}}{\partial x} & \frac{\partial f^{(i)}_{TDoA,n}}{\partial y} & \frac{\partial f^{(i)}_{TDoA,n}}{\partial z} \end{bmatrix}, \tag{11}$$

$$x = \begin{bmatrix} x \\ y \\ z \end{bmatrix}, x^{(i)} = \begin{bmatrix} x^{(i)} \\ y^{(i)} \\ z^{(i)} \end{bmatrix}.$$

Substituting (10) into (6) gives the following linear system of equations with regard to the $(\mathbf{x}–\mathbf{x}^{(i)})$:

$$\mathbf{D}^{(i)}\left(\mathbf{x}-\mathbf{x}^{(i)}\right)+\mathbf{e}=\mathbf{b}^{(i)}, \tag{12}$$

where $\mathbf{b}^{(i)}$ describes the difference between the observation vector $\mathbf{r}$ and the vector $\mathbf{f}$ estimated at the point $(x^{(i)}, y^{(i)}, z^{(i)})$.

$$\mathbf{b}^{(i)}=\mathbf{r}-\mathbf{f}\left(x^{(i)}, y^{(i)}, z^{(i)}\right). \tag{13}$$

B. Gauss-Newton Process

A Minimum Variance Unbiased (MVU) estimator exists if the error vector $\mathbf{e}$ in (12) has a Gaussian Probability Density Function (PDF) with zero mean and covariance matrix $\mathbf{C}$ [23]. Therefore, $(\mathbf{x}–\mathbf{x}^{(i)})$ can be found [24] as:

$$\mathbf{x}-\mathbf{x}^{(i)}=\left(\left(\mathbf{D}^{(i)}\right)^{T}\mathbf{C}^{-1}\mathbf{D}^{(i)}\right)^{-1}\left(\mathbf{D}^{(i)}\right)^{T}\mathbf{C}^{-1}\mathbf{b}^{(i)} \tag{14}$$

Ultimately by using (14), an iterative equation can be written to update vector $\mathbf{x}$ based on its previous estimate:

$$\mathbf{x}^{(i+1)}=\mathbf{x}^{(i)}+\left(\left(\mathbf{D}^{(i)}\right)^{T}\mathbf{C}^{-1}\mathbf{D}^{(i)}\right)^{-1}\left(\mathbf{D}^{(i)}\right)^{T}\mathbf{C}^{-1}\mathbf{b}^{(i)} \tag{15}$$

Here $\mathbf{C}^{-1}$ is a $3N-1\times 3N-1$ inverse covariance matrix of vector $\mathbf{e}$. The error in measurements comes from the reliability of LOS and NLOS identification. By measuring $\Lambda^2_{l,m}$ after beam determinations, which is the channel impulse response power of the l^{th} gNB and the m_{th} time domain path from the total number of channel time domain paths N^{th}_m, used in the channel estimation, we have the test statistics u_l for the first path channel impulse response power $\Lambda^2_{l,1}$ from l^{th} gNB:

$$u_l=\Lambda^2_{l,1}/\sum_{m=1}^{N_m}\Lambda^2_{l,m} \tag{16}$$

Therefore, we assume that the first received path in channel impulse response in time domain from each gNB corresponds to the LOS channel component. We take $\mathrm{C}^{-1}_{l,l}=1$ for LOS if u_l exceeds the threshold, otherwise, $\mathrm{C}^{-1}_{l,l}=0$ for NLOS.

$$C^{-1}_{l,l}=F\left(u_l\right)=\begin{cases}1 & \text{if} \quad u_l>\gamma \\ 0 & \text{if} \quad u_l\le\gamma\end{cases} \tag{17}$$

Where the threshold γ=0.5 gives the best trade-off between the probability of NLOS detection and false alarm. The resulting equation (15), starting from an initial guess $\mathbf{x}^{(0)}$, converges after a few iterations as shown in figure 7, and the vector $\mathbf{x}^{(i+1)}$ found at the last iteration is used as an estimate of the UE coordinates (x, y, z).

VI. Simulation Setup

To evaluate the proposed algorithm's performance, we created a simulation environment in Matlab, based on the 3gpp standard indoor scenario with a map-based channel [25], which represents a $60m \times 120m \times 10m$ factory hall.

8 gNBs with known locations are installed above the clutters which improves the availability of LOS. There are 12 metal clutters with various dimensions, scattered on the ground. The clutters may block the LOS between the gNBs and the UE as well as reflect the downlink rays. UE can have a random horizontal position with a standard height of 1.5 m. Each of the gNBs transmits the DL-PRS with the configuration in table I. To show the effect of transmitter antenna array size on the final positioning result, two different sizes of 2×2, and 4×4 are used.

Parameter	**Value**
Channel model type	InF (Indoor Factory)
Factory size	60x120x10
DL-PRS (carrier frequency, bandwidth)	26 GHz, 400MHz
Sub-carrier spacing	120 KHz
Total gNB TX power	24 dBm
gNB antenna configuration 1	2x2, dz = dy = λ/2
gNB antenna configuration 2	4x4, dz = dy = λ/2
gNB antenna radiation pattern	single sector, vertical
gNB antenna height	8 m
UE antenna configuration	Single element
UE antenna radiation pattern	omni-directional
UE antenna height	1.5 m
numBeams	4 or 16
PRSResourceSetPeriod	numBeams
NumRB	264 (400 MHz)
NumPRSSymbols	12 per slot
CombSize	12
NPRSID	[0,4095]
REOffset	NPRSID - 1

TABLE I
SIMULATION PARAMETERS

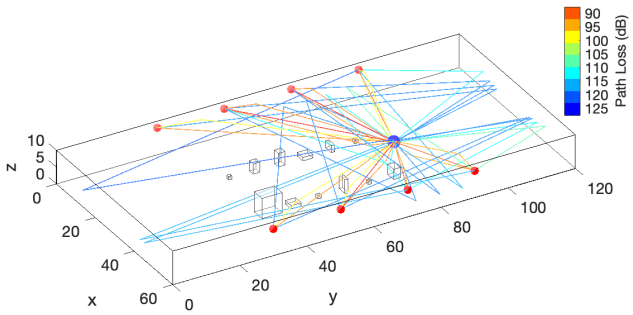

Fig. 4. Factory hall simulation environment

A. Propagation Model

Our propagation model consists of a deterministic and a probabilistic part. First, we compute the delays and average amplitudes of all the multi-path components based on a site-specific ray-tracing model. Second, we use these parameters in a Clustered Delay Line (CDL) channel model to generate multiple instances of the channel.

1) Ray Tracing

This method employs ray tracing to display and compute propagation pathways with surface geometry provided by the 'Map' attribute. Each displayed propagation path is color-coded according to the received power (dBm) or path loss (dB) along the path. The ray tracing analysis includes surface reflections but does not include effects from diffraction, refraction, or scattering

B. Channel Model

To obtain the channel-impaired signal we pass the transmit signal through a Clustered Delay Line (CDL) multi-input multi-output (MIMO) link-level fading channel. CDL-delay profile is configured using the ray-tracing propagation model outputs including path delay and path gain, angle of departure, and arrival. The first path follows a Ricean fading distribution which can point to LOS and the other paths follow a Rayleigh fading distribution coming from multipath propagation.

VII. Results

Figures 4 and 5 demonstrate the Cumulative Distribution of horizontal and vertical error for 100 randomly chosen user locations. TDoA and AoD positioning methods were employed both independently and jointly. As the results reveal, TDoA may achieve satisfactory horizontal precision, whereas AoD leads to proper vertical accuracy. The joint position estimation approach, on the other hand, produces a precise estimation of user coordinates in both directions. The graphs also show how a bigger antenna array enhances accuracy. This improvement is due to more beams produced by a bigger antenna array, as well as enhanced transmitter angle coverage and beamforming.

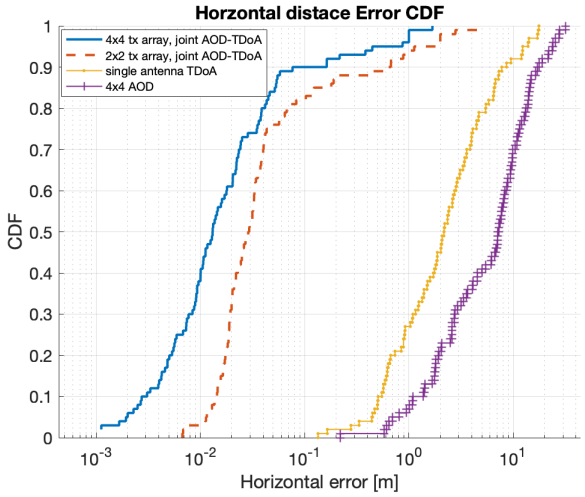

Fig. 5. Horizontal positioning error

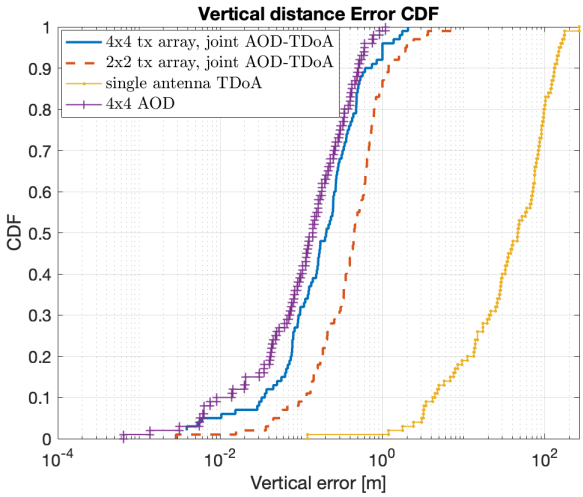

Fig. 6. Vertical positioning error

Table II illustrates an analytical comparison between two positioning results based on Horizontal Root Mean Square Error (HRMSE) and Vertical Root Mean Square Error (VRMSE) where M is the number of user positions in simulations. In this paper, M = 100.

$$\text{HRMSE} = \sqrt{\frac{1}{M}\sum_{j=1}^{M}\left(\text{HPE}_i^2\right)}, \text{VRMSE} = \sqrt{\frac{1}{M}\sum_{j=1}^{M}\left(\text{VPE}_i^2\right)} \quad (18)$$

Methods and configurations	**HRMSE** [m]	**VRMSE** [m]
TDoA, Single TX antenna	1.8814	7.7363
AOD, 4×4 TX array	2.8754	0.4571
Joint TDoA-AOD, 2×2 TX array	0.4721	0.8119
Joint TDoA-AOD, 4×4 TX array	0.2909	0.5577

TABLE II
RMSE COMPARISON

Despite the mean squared error for vertical and horizontal being less than 1m in multi-antenna configurations, a larger antenna array enhances accuracy even further.

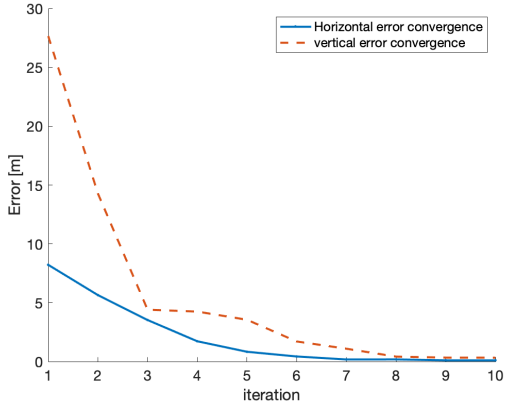

Fig. 7. Gauss-Newton process error convergence

VIII. Conclusion

In this paper, we derived a joint Downlink Angle of Departure (DL AoD) and Downlink Time Difference of Arrival (DL TDoA) positioning algorithm for UE self-position estimation in 3GPP 5G NR release 16 mm-wave systems. The algorithm exploits the newly introduced possibility to broadcast assistance data to the UE that includes information about the exact location of the antennas and the angles of departure corresponding to different beam indices. The DL TDoA estimation exploits the Downlink Positioning Reference Signal (DL-PRS) while the DL AoD is deduced from the index of the serving beam at the gNB. The proposed algorithm uses a LOS/NLOS link classification to filter out NLOS measurements that have a negative impact on the estimation performance. Simulations are carried out by a ray-tracing propagation model in an Indoor Factory Hall (InF-H) map-based channel model. We show that in a mm-wave scenario with 8 gNBs each using $4 \times 4 = 16$ element antenna array and 400MHz of channel bandwidth, the presented joint AoD-TDoA algorithm can achieve horizontal accuracy of $<$1m in 99% of the cases and $<$10cm in 90% of the cases.

Acknowledgment

The work included in this paper has been supported by the European Space Agency Navigation Innovation and Support Programme (NAVISP) through the project HOP-5G. The view expressed herein can in no way be taken to reflect the official opinion of the European Space Agency. The authors would like to thank Rakesh Mundlamuri for producing the indoor map of this paper's simulation.

References

[1] D. Wang, G. Hosangadi, P. Monogioudis, and A. Rao, "Mobile device localization in 5G wireless networks," International Conference on Computing, Networking and Communications (ICNC), 2019.

[2] T.-K. Le and N. Ono, "Closed-form and near closed-form solutions for TOA-based joint source and sensor localization," IEEE Transactions on Signal Processing, vol. 64, 2016.

[3] N. H. Nguyen and K. Dog anc ay, "Optimal geometry analysis for multistatic TOA localization," IEEE Transactions on Signal Processing, vol. 64, 2016.

[4] J. A. del Peral-Rosado, R. Raulefs, J. A. Lo pez-Salcedo, and G. Seco-Granados, "Survey of cellular mobile radio localization methods: From 1G to 5G," IEEE Commun. Surveys Tuts., vol. 20, pp. 1124–1148, 2018.

[5] P. Tarrio, A. M. Bernardos, J. A. Besada, and J. R. Casar, "A new positioning technique for RSS-based localization based on a weighted least squares estimator," IEEE International Symposium on Wireless Communication Systems, 2008.

[6] T. Stoyanova, F. Kerasiotis, C. Antonopoulos, and G. Papadopoulos, "RSS-based localization for wireless sensor networks in practice," 9th International Symposium on Communication Systems, Networks and Digital Sign (CSNDSP), 2014.

[7] D. Munoz, C. Vargas, R. Enriquez-Caldera, and F. B. Lara, Position Location Techniques and Applications. Academic Press, 2009.

[8] S. Wong, R. Jassemi-Zargani, D. Brookes, and B. Kim, "A geometric approach to passive target localization," ST Organization, 2017.

[9] Y.T.ChanandK.C.Ho,"A simple and efficient estimator for hyperbolic location," IEEE Transactions on Signal Processing, vol. 42, no. 8, pp. 1905–1915,, 1994.

[10] Y. Huang, J. Benesty, G. W. Elko, and R. M. Mersereau, "Real-time passive source localization: a practical linear-correction least-squares approach," IEEE Transactions on Speech and Audio Processing, vol. 9, no. 8, pp. 943–956, 2001.

[11] K. W. Cheung, H. C. So, W. K. Ma, and Y. T. Chan, "A constrained least squares approach to mobile positioning: algorithms and optimality," Hindawi Publishing Corporation EURASIP Journal on Applied Signal Processing, 2006.

[12] K. Yang and J. An, "Constrained total least-squares location algorithm using time-difference-of-arrival measurements," IEEE Transactions on Vehicular Technology, vol. 59, no. 3, 2010.

[13] W. Chen, S. He, Q. Xu, J. Ren, Y. Huang and L. Yang, "Positioning Algorithm and AoD Estimation for mmWave FD-MISO System," 2018 10th International Conference on Wireless Communications and Signal Processing (WCSP), 2018, pp. 1-6, doi: 10.1109/WCSP.2018.8555713.

[14] 3GPP TS 38.305, 5G; NG Radio Access Network (NG-RAN); Stage 2 functional specification of User Equipment (UE) positioning in NG-RAN

[15] 3GPP TS 37.355, LTE; 5G; LTE Positioning Protocol (LPP)

[16] 3GPP TS 38.211 5G; NR; Physical channels and modulation

[17] S. He, J. Wang, Y. Huang, B. Ottersten, and W. Hong, "Codebook-Based Hybrid Precoding for Millimeter Wave Multiuser Systems," IEEE Transactions on Signal Processing, vol. 65, no. 20, pp. 5289- 5304, Oct.15, 15 2017.

[18] 3GPP TR 38.802. "Study on New Radio access technology physical layer aspects." 3rd Generation Partnership Project; Technical Specification Group Radio Access Network.

[19] A. Abdi, C. Tepedelenlioglu, M. Kaveh and G. Giannakis, "On the estimation of the K parameter for the Rice fading distribution," in IEEE Communications Letters, vol. 5, no. 3, pp. 92-94, March 2001, doi: 10.1109/4234.913150.

[20] 3GPP TS 38.215. " NR Physical layer measurements." 3rd Generation Partnership Project; Technical Specification Group Radio Access Network.

[21] J. . -J. van de Beek, O. Edfors, M. Sandell, S. K. Wilson and P. O. Borjesson, "On channel estimation in OFDM systems," 1995 IEEE 45th Vehicular Technology Conference. Countdown to the Wireless Twenty-First Century, 1995, pp. 815-819 vol.2, doi: 10.1109/VETEC.1995.504981.

[22] W. H. Foy, "Position-location solutions by Taylor-series estimation," IEEE Trans. Aerosp. Electron. Syst., vol. AES-12, pp. 187-194, March 1976.

[23] S. M. Kay, Fundamentals of Statistical Signal Processing – Detection Theory, vol. 2. Englewood Cliffs, NJ: Prentice-Hall, 1998.

[24] S. Sosnin, A. Lomayev and A. Khoryaev, "DL-AOD Positioning Algorithm for Enhanced 5G NR Location Services," 2021 International Conference on Indoor Positioning and Indoor Navigation (IPIN), 2021, pp. 1-7, doi: 10.1109/IPIN51156.2021.9662638.

[25] 3GPP TR 38.901 "Study on channel model for frequencies from 0.5 to 100 GHz".